JOURNAL OF GEOPHYSICAL RESEARCH, VOL. 114, C09009, doi:10.1029/2008JC005235, 2009

Long-range temporal correlations of ocean surface currents

Yosef Ashkenazy[1] and Hezi Gildor[2]

Received 9 December 2008; revised 14 April 2009; accepted 7 May 2009; published 10 September 2009.

[1] We study the temporal correlations of sea surface currents at the Gulf of Eilat (also known as Gulf of Aqaba) and find long-range temporal correlations, from a timescale of several hours to a timescale of several months. This is done using the Fourier transform and the Detrended Fluctuation Analysis methods. We also find weak volatility correlations that indicate nonlinearity of surface currents. We use the time-dependent surface Ekman layer model to test whether the source of these correlations is the wind. It is found that the wind by itself actually leads to stronger temporal correlations than observed, as well as enhanced diurnal periodicity; other nonlinear terms as well as tides, convection, and spatial variability may weaken the temporal correlations imposed by the wind. Our results show significant spatial variability of correlation exponents even in this small region (6 × 10 km); in addition, stronger correlations are observed during winter.

Citation: Ashkenazy, Y., and H. Gildor (2009), Long-range temporal correlations of ocean surface currents, *J. Geophys. Res.*, *114*, C09009, doi:10.1029/2008JC005235.

1. Introduction

[2] Temporal long-range correlations have been detected in many geophysical time series [e.g., *Mandelbrot and Wallis*, 1969], covering timescales from minutes [e.g., *Govindan and Kantz*, 2004] to hundreds of thousands of years [e.g., *Pelletier*, 1997; *Ashkenazy et al.*, 2003a; *Huybers and Curry*, 2006]. These include wind data [*Schulz et al.*, 2001; *Kocak*, 2008; *Roman et al.*, 2008], temperature records [*Govindan et al.*, 2002; *Fraedrich and Blender*, 2003; *Fraedrich et al.*, 2004; *Bunde et al.*, 2004], river fluxes [*Hurst*, 1951; *Turcotte and Greene*, 1993; *Tessier et al.*, 1996; *Pandey et al.*, 1998; *Livina et al.*, 2003], precipitation [*Kantelhardt et al.*, 2006] etc. The majority of these examples are associated with the atmosphere or with land surface while the ocean variables, in spite of their importance to the climate system, have received only minor attention from this prospective. Recent remote sensing instruments and techniques can provide continuous temporal and spatial resolution data from the ocean surface. The study of such data sets may improve our understanding of the ocean-atmosphere coupling and of the mixing processes' parameterization used in general circulation models.

[3] Here we study high temporal and spatial resolution ocean surface (approximately the upper half meter) current data set. The temporal resolution is half an hour and the spatial resolution is approximately 300 m, while the time span of the studied period is one year, from 1 October 2005 to 30 September 2006. The currents were measured using high-frequency (HF) radar (see more details below) at the northern end of the Gulf of Eilat and they cover an area of ~6 km × ~10 km (Figure 1). The aims of this study are (1) to report the temporal long-range correlations of surface currents and (2) to investigate to what extent the wind's action underlies these correlations. Our results indicate that the wind by itself is expected to bring upon an even stronger correlations than the observed ones while other factors like spatial variations (e.g., bathymetry), tides, convection processes, and other linear/nonlinear factors (e.g., advection) act to weaken these correlations. Moreover, we show that while the wind seems to exhibit linearity, the surface current exhibits nonlinearity as reflected by volatility correlations. We also show that in spite of the relatively small studied area, there are significant spatial differences in the correlation properties of the surface currents.

[4] The northern terminus of the Gulf of Eilat is a nearly rectangular, deep (~700 m), and semienclosed basin in the northeast region of the Red Sea. The desert mountains surrounding the Gulf of Eilat act like a tunnel roughly elongated along the South-North axis and lead to the nearly persistent northerly wind along its main axis [*Berman et al.*, 2003]; for the time period of October 2005 to September 2006 the wind blew 9%, 45%, and 12% of the time from the N, NNE and NE directions, while during 34% of the time it blew more or less uniformly from all other directions. The circulation in the gulf has three main driving forces: winds, tides, and buoyancy. The tides are dominated by the semidiurnal peak associated with the water flux through the Straits of Tiran [*Genin and Paldor*, 1998; *Monismith and Genin*, 2004; *Manasrah et al.*, 2006]. The tidal signal mainly affects the upper ocean layer in the gulf and thus is much stronger during summer (when the thermocline is around 200 m) than during winter (when the water column is mixed down to a few hundreds meters) [*Monismith and Genin*, 2004; *Berman et al.*, 2003].

[5] Surface currents in the northern Gulf of Eilat are measured by two 42 MHz SeaSonde HF radar systems

[1]Department of Solar Energy and Environmental Physics, BIDR, Ben-Gurion University, Midreshet Ben-Gurion, Israel.
[2]Department of Environmental Sciences and Energy Research, Weizmann Institute of Science, Rehovot, Israel.

0148-0227/09/2008JC005235$09.00

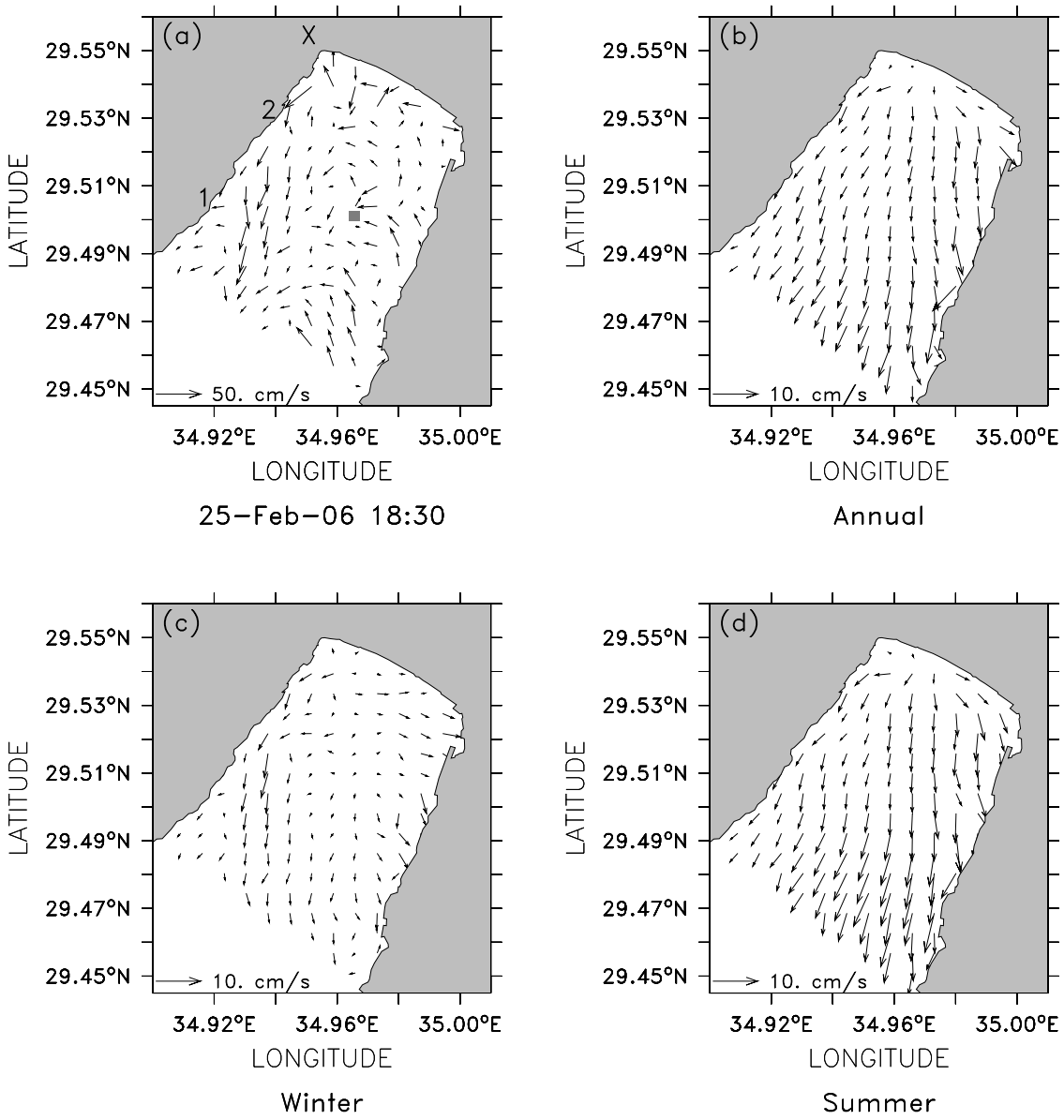

Figure 1. (a) A typical example of surface current field recorded at the Northern Gulf of Eilat on 25 February (18:30) 2006. The numbers "1" and "2" indicate the locations of the two HF radar stations, while cross (×) indicates the location of the meteorological station from which we use the wind data. The gray square indicates the location of the time series shown in Figure 2. (b) Annual mean current field (October 2005 to September 2006). (c) Same as Figure 1b for the winter time period (January to March 2006). (d) Same as Figure 1b for the summer period (July to September 2006). In the presented current fields, we skip every second grid point in both directions to allow a better visualization.

since August 2005; the locations of the HF radars as well as the coastline of the gulf are shown in Figure 1. Each station measures the current component toward or away of the antenna, called ''radial''. There is one SeaSonde at the Inter-University Institute in Eilat and another station at the Port of Eilat. In order to approximate the current vector at a certain point, we need to have radials measurements from both stations and the two should observe this patch of water from different angles. Ideally, we want an angle of about 90 degrees between the two radials and, in any case, at least 15 degrees [*Barrick et al.*, 1985; *Barrick*, 2002]. In addition to geometric considerations, such as the distance from the radar stations and the angle between the radials, the accuracy of the measurement is also subject to other factors such sea conditions. When the amplitude of the surface gravity waves is too small, as is often the case in the northernmost few hundreds meters of the domain, there are gaps in the data. For a detailed description regarding the radar measurements and processing of the data, including comparison to some observations, see studies by *Gildor et al.* [2009] and *Lekien and Gildor* [2009]. The observed surface current field often exhibits a complex pattern as shown in Figure 1a, with mostly northerly currents and weaker currents during winter.

[6] The work is presented as follows. In section 2 we briefly describe the techniques that are used to quantify the

long-range temporal correlations. These include the Fourier transform, the Detrended Fluctuation Analysis (DFA), volatility long-range correlations, as well as surrogate data tests that are used to validate and estimate the uncertainty of the observed correlations. The results are presented in section 3. We then use a simple, time-dependent surface Ekman layer model, to study the contribution of the winds to the observed correlations (section 4). A summary and discussion is followed (section 5).

2. Methods

[7] Below we briefly summarize the techniques that we use to analyze the surface current data. These include Fourier transform, Detrended Fluctuation Analysis, volatility correlations, and surrogate data tests to validate a power law correlations of time series and the nonlinearity of time series. Readers familiar with these methods can skip to section 3.

2.1. Fourier Transform

[8] A basic way to estimate long-range temporal correlations of a time series is through the autocorrelation function [e.g., *Makse et al.*, 1996; *Kalisky et al.*, 2005]. The autocorrelation function is related to the Fourier power spectrum; if the autocorrelation function decays as a power law, $A(\tau) \sim \tau^{-\gamma}$, the power spectrum also decays as a power law, $P(f) \sim f^{-\beta}$ where $\beta = 1 - \gamma$ and $0 < \gamma < 1$. $\beta = 0$ indicates white noise (i.e., all frequencies are equally important), $\beta = 2$ indicates red noise (i.e., the low frequencies are dominant) while $\beta = -2$ indicates blue noise (i.e., the high frequencies are dominant). The Fourier transform technique has the advantage of efficient computation and a wider range of scaling exponent β, that is, it is possible to detect scaling exponents that are larger than one or smaller than zero (unlike the autocorrelation correlations technique that is limited between $0 < \gamma < 1$). In addition, significant periodicity in a time series (like the daily periodicity) may drastically affect the autocorrelation function (and other techniques like the DFA described below) as the periodicity may be smeared over a range of scales.

[9] It is possible to estimate the power exponent (if it exists) from a linear plot or from a log-log plot. The latter choice is more suitable for the estimation of scaling (power law) exponent since it provides evenly spaced points in logarithmic scale. The presence of significant periodicity in the power spectrum only slightly affects the estimation of the scaling exponent since it is not smeared over a range of frequencies. We thus estimate the scaling exponent β from a log-log plot of the power spectrum.

2.2. Detrended Fluctuation Analysis (DFA)

[10] The estimation of the power law scaling exponent using Fourier transform technique may be affected by trends that often exist in natural time series [*Peng et al.*, 1994, 1995]. In our particular example, the seasonal variations of the surface currents may look like a long-range correlated time series. The DFA technique aims to overcome such an effect of trends. The DFA procedure can basically be described as follows [*Peng et al.*, 1994, 1995; *Kantelhardt et al.*, 2002]: the time series is considered as "steps" of a random walk. The time series is integrated, which results in the "profile" of the random walk. Thus, for example, the standard deviation of a profile of a white noise will grow like the square root of the number of steps and the corresponding scaling DFA (or Hurst) exponent will be $\alpha = 0.5$. Then, for each segment (window scale) in the time series a polynomial function is fitted and subtracted from the profile. This is done to exclude trends that are not necessarily associated with the power law characteristics of the signal. The fluctuation function provides the mean deviations around the fitted polynomial function. This procedure is repeated for various window scales. In the case of long-range correlated time series, the scaling exponent α can be estimated from a log-log plot of the fluctuation function $F(n)$ versus the window scale, n. The relation between the Fourier spectrum scaling exponent β and the DFA scaling exponent α is $\beta = 2\alpha - 1$.

[11] As mentioned in the previous subsection, when the time series has a significant periodic component, the estimation of the scaling exponent may be problematic since such periodicity may be smeared over many window scales. For the case of surface currents, the diurnal periodicity is weak and does not result in serious artifacts. Yet, to be cautious, we present both, the Fourier transform and the DFA scaling exponents.

[12] In many cases, the Fourier transform scaling curves (as well as the DFA curves) have "crossovers", i.e., have different scaling exponents for different frequency regimes. Usually, for geophysical time series like the ones we handle here, the scaling exponent is larger for the higher frequencies (small scales) due to the relatively strong temporal correlations of a few days of weather systems. In that case, it is necessary to estimate the scaling exponent for these different regimes. The time series we study here do not seem to have such crossovers and thus we present a single scaling exponent for the entire frequency (or window scale) regime.

2.3. Volatility Correlations

[13] It is possible to gain some information regarding the nonlinearity of the time series by studying its "volatility" correlations [*Ashkenazy et al.*, 2001, 2003b; *Kalisky et al.*, 2005]. We define nonlinearity with respect to the Fourier phases: when the statistical properties of the time series remain unchanged after randomizing its Fourier phases the time series is defined as linear, while otherwise it is defined as nonlinear [*Schreiber and Schmitz*, 1996, 2000]. This is motivated by the fact that (linear) autoregressive moving average (ARMA) processes are independent of the Fourier phases. By volatility we refer to temporal correlations in time series of the absolute values of the increment time series which reflect the way that fluctuations (either positive or negative) are clustered together [*Ashkenazy et al.*, 2001, 2003b; *Kalisky et al.*, 2005]. It has been shown that long-range volatility correlations may be linked to nonlinearity and multifractality of time series [*Ashkenazy et al.*, 2001, 2003b; *Kalisky et al.*, 2005]. It is necessary to validate that indeed the volatility correlations are linked to the Fourier phases and not to other factors like the probability distribution function, using surrogate data tests described in the next subsection.

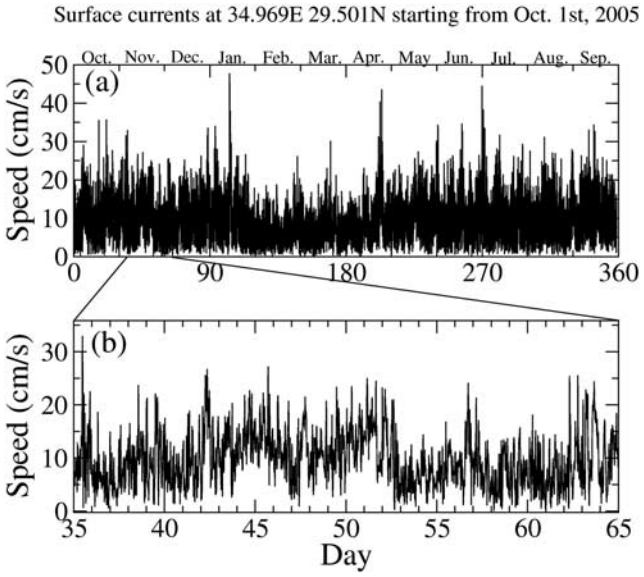

Figure 2. (a) An example of a time series of surface current speed (in cm/s) as measured by the HF radar. The time series spans 1 year starting 1 October 2005 and represents the mean surface current of a grid point of ≈300 m × ≈300 m located at 34.969°E and 29.501°N (indicated by a gray square in Figure 1). Note that in this location, the accuracy and coverage of the measurements are near optimal. (b) An enlargement of the time series presented in Figure 2a.

2.4. Surrogate Data Tests

[14] To asses the uncertainty of the estimated scaling exponent and to study the nonlinearity of the volatility correlations we use two surrogate data tests.

[15] 1. By randomly exchanging pairs of points of the time series, the probability distribution function of the time series remains unchanged while the temporal correlations are destroyed. The mean and the standard deviation of the scaling exponent of the randomized time series may indicate how significant is the observed scaling exponent and what are the error bars due to the finite size of the time series and due to the probability distribution.

[16] 2. It is possible to generate surrogate time series from the original time series such that the probability distribution function and the Fourier amplitude are kept almost as the original ones while the Fourier phases are randomized [*Schreiber and Schmitz*, 1996, 2000]. Using this surrogate data technique, it is possible to reject a null hypothesis regarding the nonlinearity of the time series since linear (ARMA) processes are independent of the Fourier phases. If a statistical measure of the original time series is significantly different than the surrogate time series ones then the null hypothesis of linearity is rejected and the time series can be considered as nonlinear.

3. Results

[17] The surface currents in the Gulf of Eilat are highly variable and at times quite complex. In Figure 1a we show an example for a snapshot of surface current field which exhibits rich spatial variability, even in such a small area. The time series of a particular location (located in front of the two stations, at a region with very few gaps in the data) is also highly variable (Figure 2); weak seasonal and daily variability is also present with reduced speeds during the winter months. This pattern is a typical.

[18] A detailed analysis of the time series shown in Figure 2 is depicted in Figure 3. We first perform a conventional Fourier transform (Figure 3a) from which it is clear that the low frequencies dominant the signal where the daily periodicity is relatively weak. This hints to long-range temporal correlations. To asses this more accurately we plot the power spectrum on a log-log plot (Figure 3b), both using linear and logarithmic binning. The logarithmic binning is more suitable for the estimation of the power law scaling exponent β. It is apparent that the scaling curves have similar slope for the different frequency regimes. We estimate the power law scaling exponent by least squares fitting the power spectrum to a power law function and obtain a power law exponent of $\beta \approx 0.7$, suggesting long-range temporal correlations. This is a typical scaling curve although grid points close to the shore may have crossovers. We estimate the scaling exponent of 20 shuffled time series of the time series shown in Figure 2a and obtain a mean exponent of -0.01 and a standard deviation of 0.05, suggesting that the long-range temporal correlations are highly significant.

[19] We repeat the calculation of the scaling exponent using the DFA method of order two (Figure 3c); that is, linear trends in the time series are excluded. We obtain a DFA exponent of $\alpha \approx 0.8$ for annual, winter (January to

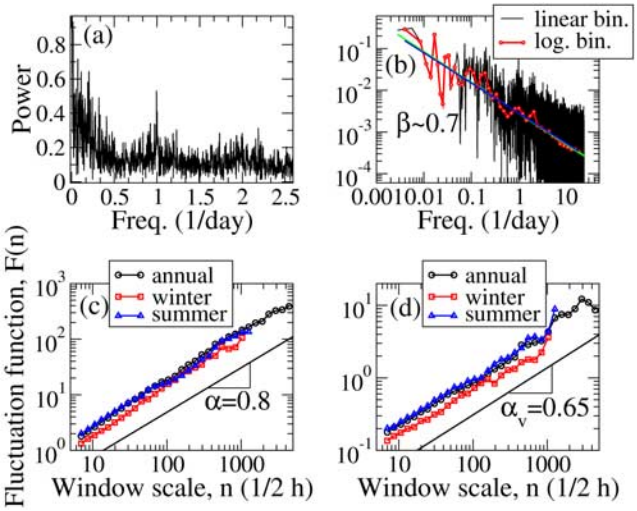

Figure 3. (a) Frequency power spectrum of the time series shown in Figure 2a. (b) Same as Figure 3a but on a log-log plot with linear binning (black curve) and logarithmic binning (red curve). The estimated power law exponent is $\beta \approx 0.7$. (c) The DFA scaling curves for the entire year (black, October 2005 to September 2006), winter (red, January to March 2006), and summer (blue, July to September 2006). The estimated DFA exponent is $\alpha \approx 0.8$ with no apparent crossover. (d) Fluctuation function curves for the volatility time series (i.e., absolute value of the increment time series). The DFA curves indicate weak volatility correlations of $\alpha_v \approx 0.65$.

March 2006), and summer (July to September 2006) time series. This value is roughly consistent with the value of the power spectrum scaling exponent $\beta = 0.7$, since theoretically $\beta = 2\alpha - 1 = 0.6$; the difference of 0.1 may be attributed to the presence of linear trends in the surface speed time series. [Below we show that the DFA exponent is consistent with the Fourier transform scaling exponent when dealing with the basin mean exponent.] Also here the DFA scaling curves do not seem to have crossovers. To estimate the significance of the scaling exponent we generate 20 shuffled time series out of the original one and obtain, as expected, a mean exponent of 0.51 and a standard deviation of 0.015. Thus, the estimated temporal correlations are highly significant and since we use the DFA they, most probably, are not associated with linear trends or seasonal variability as on the scales we consider here (days to months) the mean seasonal cycle appears as linear curves.

[20] Finally we estimate the volatility correlations (Figure 3d) using the DFA method. Here the temporal correlations are marginal and the scaling exponent is $\alpha_v \approx 0.65$ indicating weak nonlinearity of the time series. Usually, such nonlinearity is expressed by clustering of large fluctuations (up or down) followed by clustering of small fluctuations which are arranged in a self-similar pattern. Such behavior may be associated with storm activity followed by days with calm winds. To asses that indeed the volatility correlations are not an artifact of the shape of the distribution, we generate 20 surrogate time series out of the original (increment) time series using the surrogate data test proposed by *Schreiber and Schmitz* [2000]. The mean volatility exponent of the surrogate time series is 0.5 and the standard deviation is 0.02, suggesting that the observed volatility correlations are significant and that the surface current time series is indeed nonlinear.

[21] Generally speaking, one would expect that the results shown in Figure 3 would be similar to other time series in nearby locations within the domain considered here (Figure 1) due to the small basin dimensions and since the atmospheric forces (like temperature and winds), which are the main driving forces of ocean circulation, vary on much longer scales. To check this hypothesis we estimate the different scaling exponents (β, α, and α_v) for each of the available grid points. The results are presented in Figure 4.

[22] We analyze the time series of an entire year (October 2005 to September 2006), winter (January to March 2006), and summer (July to September 2006). We present (1) the Fourier power spectrum scaling exponent, β, that was estimated based on logarithmic binning curves, (2) the DFA (of order two) scaling exponent, α, and (3) the volatility scaling exponent α_v. A summary of the basin mean and standard deviation of the different exponents is given in Table 1. The surface currents are long-range correlated with Fourier power spectrum exponent $\beta \approx 0.7$ and DFA exponent $\alpha \approx 0.8$. The correlations are stronger during the winter and weaker during the summer. To estimate the significance of the exponents we generate 20 shuffled time series for each of the grid points and estimate the exponents. We obtain mean Fourier power spectrum exponent of 0 and standard deviation that is less than 0.12, and for the DFA we obtain a mean exponent of 0.5 and a standard deviation that is less than 0.03. These values indicate that the measured correlation exponents are highly significant compare to the exponents of the shuffled time series, thus indicating long-range correlations. The similarity between the β and α exponents, both spatially (Figure 4) and through the relation $\beta = 2\alpha - 1$ (Table 1), indicates that the effect of trends on the estimation of the exponents is small and that the weak daily periodicity does not really affect the estimation of the scaling exponents.

[23] The spatial pattern of the β and α scaling exponents is, in some cases, unique. More specifically, during the winter time, the southern part has a larger exponent than the northern part. There is a kind of ''front'' parallel to the north-western to south-eastern axis. The origin of this pattern is not clear to us. During the summer the situation is different and the eastern part of the gulf seems to have a larger exponent than the western part. Generally speaking, the most northern region tends to have lower exponent values. This region is the shallowest region of the gulf with a relatively gradual slope. In addition, the HF radar coverage in this region is relatively poor (because when the wind blow from the north, the waves are too weak in that region) and most values there are derived using the Open-boundary Modal analysis method applied to this region [*Lekien and Gildor*, 2009]. We speculate that such shallow region is also more drastically and readily affected by buoyancy fluxes (as this is the coldest region in the gulf [*Biton et al.*, 2008]) and thus is more erratic and closer to white noise, as the nature of this force; hence the lower exponent values.

[24] For the volatility scaling exponent the situation is a bit different. While the volatility correlations are moderate and the exponent is $\alpha_v \approx 0.65$, there are no substantial differences between the summer and winter (Figure 4 and Table 1). Still, the volatility correlations, as expressed by the volatility scaling exponent α_v, are somehow weaker during the summer, as for the Fourier and DFA scaling exponents, α and β. We validate that indeed the volatility correlations indicate nonlinearity by generating 20 surrogate time series for each of the available grid points, for which the Fourier phases are random but the probability density function and the Fourier power spectrum remain almost unchanged. We apply this for the increment time series of the surface speed current [see *Ashkenazy et al.*, 2003b]. We then measure the volatility scaling exponent of the surrogate time series using the DFA technique. We find that the mean volatility exponent is 0.494 and that the standard deviation is less than 0.054, significantly lower than the measured volatility exponent of 0.65. The volatility correlations thus represent nonlinearity of the underlying process. Similar nonlinearity has been found in other climate variables [e.g., *Bartos and Janosi*, 2006; *Govindan et al.*, 2003]. The spatial pattern of the volatility exponent α_v is not unique.

4. Time-Dependent Ekman Layer Model

[25] As mentioned above, there are three main factors/forces that may affect the circulation in the Gulf of Eilat: (1) wind, (2) tides, and (3) buoyancy fluxes. Since we are dealing with surface currents, winds are likely to have the largest influence. While winds are weaker during the winter (Figure 5a), a convection process (deep water formation) is active during the winter [*Genin and Paldor*, 1998; *Biton et al.*, 2008]; tides are more dominant during the summer due to the shallower thermocline [*Monismith and Genin*, 2004]. While convection and tides act on at least several tens of

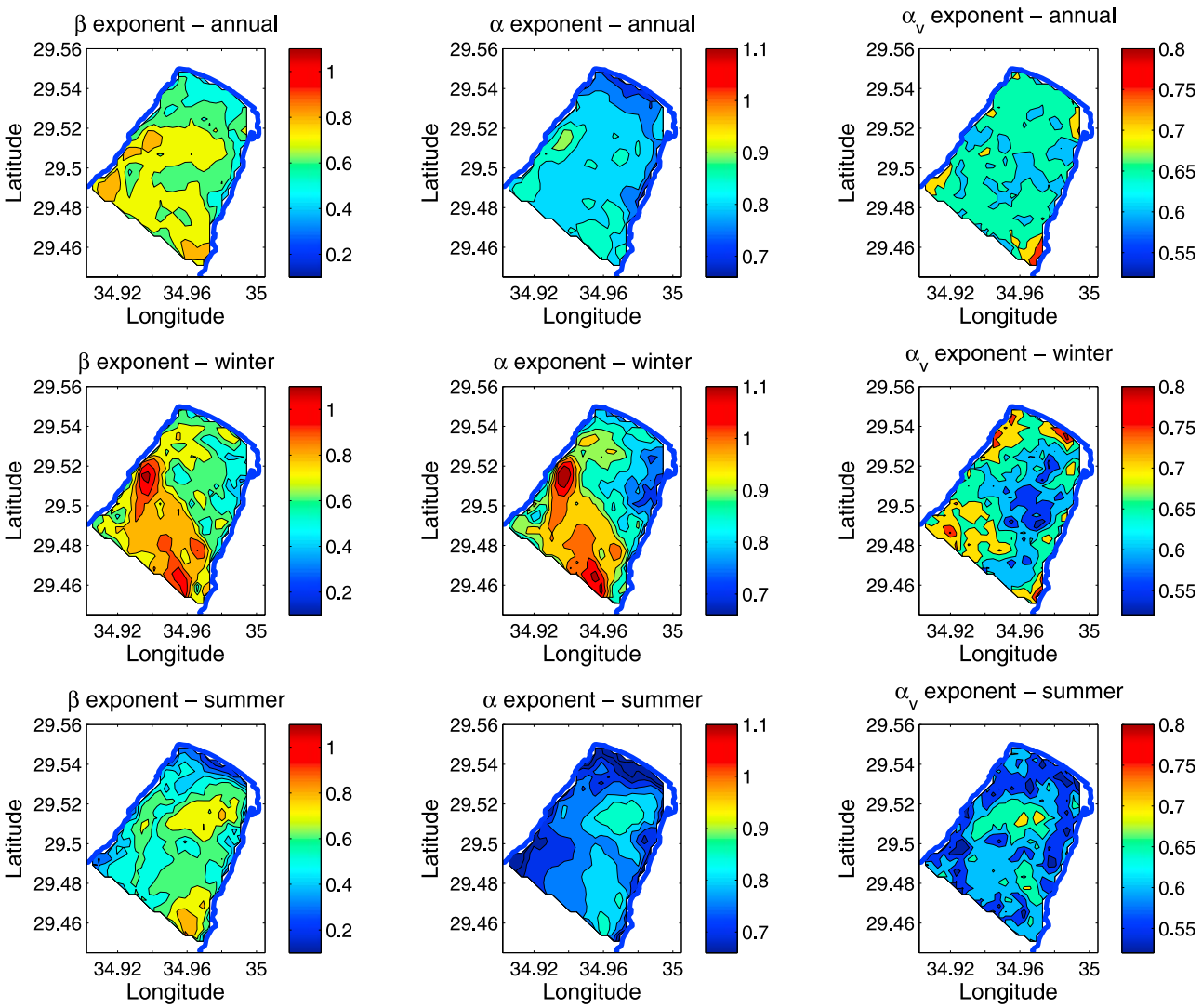

Figure 4. A summary of the scaling exponents of surface current speed. The *x*/*y* axis denotes the longitude/latitude. (left) Fourier transform scaling exponent β. (middle) DFA scaling exponent α. (right) Volatility scaling exponent α_v. Scaling exponents of the (top) annual (1 October 2005 to 30 September 2006), (middle) winter (1 January 2006 to 31 March 2006), and (bottom) summer (1 July 2006 to 30 September 2006) time period.

meters of depth, the wind's action is maximal at the surface and decreases exponentially with depth [*Ekman*, 1905; *Gill*, 1982]. We thus concentrate in the following on the wind action as the source of the observations reported in the previous section.

[26] *Ekman* [1905] studied the effect of winds on the upper (and lower) layer of the ocean and showed that surface currents are oriented to the right of the wind (in the Northern Hemisphere, NH), that the currents' speed decreases exponentially with depth, and that the entire transport due to wind is oriented 90 degrees to the right of the wind (in the NH). The current vector rotates anticyclonically (clockwise in the NH) with depth. The Ekman model has two independent variables, time (t) and depth (z) where the model has analytical time-dependent and time-independent solutions for constant winds [*Ekman*, 1905]. We numerically solve the time-dependent Ekman model that is forced by the observed winds presented in Figure 5a.

[27] In particular, we solve the following set of equations:

$$\frac{\partial u}{\partial t} - fv = \nu \frac{\partial^2 u}{\partial z^2}, \tag{1}$$

$$\frac{\partial v}{\partial t} + fu = \nu \frac{\partial^2 v}{\partial z^2}, \tag{2}$$

Table 1. Summary of the Scaling Exponents β, α, and α_v[a]

Exponent	Annual	Winter	Summer
β	0.69 ± 0.09	0.74 ± 0.14	0.59 ± 0.13
$(\beta + 1)/2$	0.845 ± 0.045	0.87 ± 0.07	0.795 ± 0.065
α	0.83 ± 0.04	0.91 ± 0.09	0.77 ± 0.06
α_v	0.67 ± 0.03	0.67 ± 0.055	0.61 ± 0.04

[a]The mean ± 1 SD of the available data is given. The DFA exponent that is calculated from the relation $\beta = 2\alpha - 1$ is also given to allow easier comparison with the DFA α exponent.

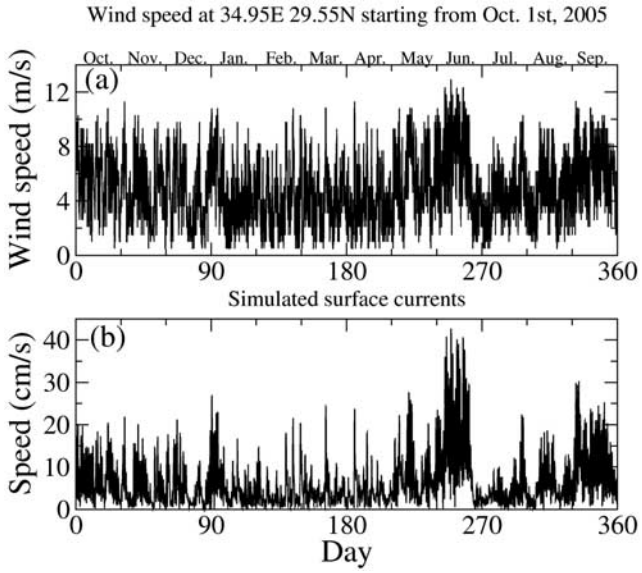

Figure 5. (a) Wind speed in m/s for the time period of October 2005 to September 2006 at 34.95°E, 29.55°N (slightly north to the Gulf of Eilat, from Eilat airport indicated by "X" in Figure 1a). (b) Simulated surface currents (in cm/s).

where u and v are the zonal and meridional ocean velocities, f is the Coriolis parameter, and ν is the eddy viscosity coefficient. Here we ignore the nonlinear advection terms, the lateral (x and y) dynamics, and the basin topography, while the density is assumed to be constant. The boundary conditions are constant current, $\bar{u}$, $\bar{v}$, at some depth H and at the surface the wind stress is related to the derivative of the surface currents through

$$\frac{\partial \vec{u}}{\partial z}|_{z=0} = \frac{\vec{\tau}}{\nu \rho_o} \tag{3}$$

where ρ_o = 1028 kg/m^3 is the water density and $\vec{\tau}$ is the wind stress vector given by

$$(\tau^x, \tau^y) = \rho_a C_D U(u_a, v_a), \tag{4}$$

where U is the wind speed (usually at 10 m height), u_a and v_a are the zonal and meridional winds, ρ_a is the air density, and C_D is the drag coefficient. The air density that we use is ρ_a = 1.3 kg/m^3 and the drag coefficient is $C_D = 10^{-3}$ for $U \leq 6.2$ m/s and $C_D = (0.6094 + 0.063U)10^{-3}$ for $U > 6.2$ m/s [after *Gill*, 1982]. The other parameters values are: ν = 0.01 m^2/s and $f = 7.16 \times 10^{-5}$ s^{-1} corresponding to the Coriolis parameter at the latitude of the Gulf of Eilat. We assume a depth of H = 50 m, a vertical resolution of Δz = 0.5 m, and integration time step of Δt = 10 s. The hourly wind data (depicted in Figure 5a) were linearly interpolated to provide the wind data at each time step. The deep ocean currents are assumed to be zero.

[28] In Figures 6a–6c we show the Fourier power spectrum of the wind and simulated surface currents, both on linear and log-log plots. The diurnal periodicity is pronounced, much more than the periodicity of the surface current presented in Figure 3a. We thus do not perform DFA to measure the scaling exponent as artifacts may arise. Several studies have reported long-range correlations of wind speed [*Schulz et al.*, 2001; *Kocak*, 2008; *Roman et al.*, 2008]. We find a similar scaling exponent for the wind speed of the Gulf Eilat, β = 0.86. The simulated surface current speed exhibits much stronger correlations with correlation exponent β = 1.25 compare to the data that has a scaling exponent of $\beta \sim 0.7$. Moreover, unlike the data which exhibits straight scaling curve (Figure 3b) the simulated current curve has crossover where the high frequencies has a larger exponent. This observation can be supported analytically (see Appendix A). Deeper currents have more pronounced crossover and thus less dominant high frequencies which end up with smoother time series (see Appendix A).

[29] The wind data does not seem to exhibit volatility correlations (Figure 6d); the power spectrum of the absolute values of the surface current speed increments is parallel to the x axis with exponent $\beta \sim 0$ indicating absence of correlations. The simulated surface current speed time series does show volatility correlations as follows from the pronounced power at the low-frequency regime. However the volatility correlations of the simulated surface currents are not indicative for nonlinearity as the NULL hypothesis of linearity is not rejected as the volatility correlations of the phase randomized data is similar to the original ones. The absence of nonlinearity of the simulated currents is expected due to the linearity of the model (equations (1), (2)).

5. Summary and Discussion

[30] We analyze the long-range correlations of surface current speed of the Gulf of Eilat. The current field is

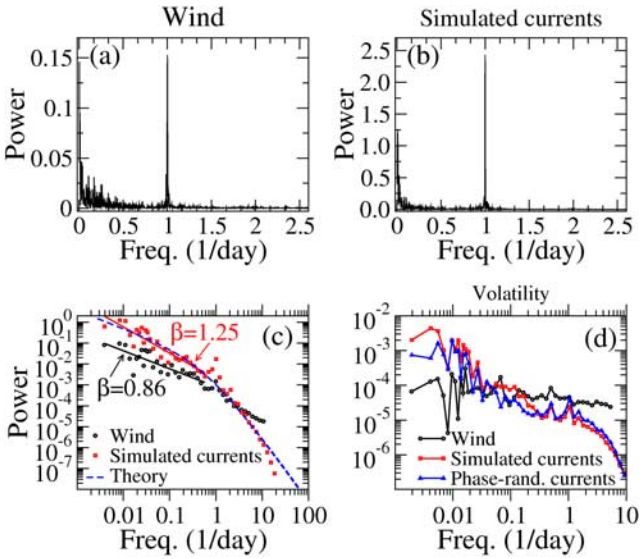

Figure 6. (a) The Fourier power spectrum of the wind speed time series shown in Figure 5a. (b) Same as Figure 6a for the simulated surface current speed shown in Figure 5b. (c) Log-log plot of the curves shown in Figures 6a and 6b and the theoretical scaling curve as developed in the Appendix A (equation (A6)). (d) Power spectrum of the absolute values of the increments of the wind speed (black), simulated surface current speed (red), and surrogate time, phase-randomized time series of the simulated currents (blue).

unique and has fine temporal (half an hour) and spatial (≈300 m) resolution. We find that the surface currents are long-range correlated and have a Fourier power spectrum scaling exponent of $\beta \sim 0.7$. The long-range correlations are from timescales of hours to several months, thus covering more than two orders of magnitudes. In addition, the surface current field posses volatility correlations that are an indication for nonlinear underlying dynamics. We show that the observed correlations are significant using surrogate data techniques.

[31] To track the source of the observed correlations we simulate upper ocean currents using a time-dependent Ekman layer model. The only forcing in this model is the wind. We find that the simulated currents of this model are much different from the observed ones as follows: (1) the diurnal periodicity of the simulated current is much more pronounced than the observed one, (2) the simulated currents are much more correlated than the observed currents, (3) the scaling curves of the simulated current exhibit crossover behavior with stronger correlations for the high frequencies while the observed currents show approximately straight scaling curves, and (4) although the simulated currents exhibit volatility correlations these are not indicative for nonlinear behavior, in contrast to the observed current for which the volatility correlations are indication for nonlinearity.

[32] It is not expected that the simulated currents will posses nonlinearity since the underlying model is linear; note that the wind-forcing is also linear by our definition for nonlinearity (Figure 6d). The differences between the linear scaling features of the observed and simulated currents suggest that other processes, in addition to the wind, may have a significant effect on the scaling properties. The convection process is, most probably, not the major one since we observe the differences both in summer and winter, while the convection process is much more significant during winter. This is also true for the tides that are more dominant during summer. Thus it might be that the nonlinear terms of the governing equations, like the advection terms, have some role in weakening the correlations and in resulting in straight scaling curves. In addition, the bathymetry and the shape of the basin may also play some role in the scaling properties. The unique pattern of the scaling exponents during winter and summer suggests that convection and tides may also weaken the correlations, although most probably less significantly than the nonlinear terms. Preliminary simulations of an atmospheric mesoscale model indicated the high spatial and temporal variability of the wind field; such variability with/without interaction with other processes may also affect the observed scaling.

[33] We observe stronger correlations during the winter. We speculate that these are due to the much deeper thermocline during winter which lead to slower response to external forcing and thus to stronger correlations. However, the convection process which is active during winter, may add noise into the system as it occurs in an erratic way when the surface temperature is cold enough to cause the sinking of surface water. Such extreme cold atmospheric events are erratic in their nature. An additional speculation is that white noise (or weakly correlated noise) is superimposed on the tidal signal; thus, in summer, when the tides are dominant the low-frequency regime is more affected by these weaker correlations to result in weaker correlations in the current speed time series while the opposite may cause stronger correlations during winter.

[34] Many natural time series exhibit long-range temporal correlations. Linear correlations may be reproduced by simple linear stochastic processes like auto regression moving average fractional Brownian motion processes. The example of surface currents discussed here suggests that nonlinear terms are involved in determining the linear scaling properties of the studied time series.

[35] Our results might be influenced to some extent by the observational technique and the method used to interpolate the data. However, this influence is most probably not very strong. In a large fraction of the domain, located in front of the two stations, the temporal coverage exceeds 90%. In addition, this region is hardly affected by the interpolated method [*Lekien and Gildor*, 2009] and the accuracy of the measurements there is optimal. Comparison of the measurements at a specific location in that region to currents measurements by an Acoustic Doppler Current Profiler (ADCP) show very good correlations [*Gildor et al.*, 2009]. Even within this region, the scaling exponents are inhomogeneous.

[36] The results reported here may be important for testing state-of-the-art ocean simulations. Our preliminary results based on ocean general circulation model show that there are large differences between the scaling properties of the measured surface currents and those simulated by the model. These differences might be due to simplified forcing fields (like taking monthly mean data instead of hourly based data) that are usually used in such models, due to simplified small-scale eddy parameterization (e.g., constant eddy coefficient in fine resolution and small-scale basins, which was shown to be incorrect in this region [*Gildor et al.*, 2009]), or due to the effect of tides that in many cases are not taken into account. When forcing the time-dependent Ekman model presented above with monthly mean wind data that are linearly interpolated for each time step we obtain currents that very slowly and linearly change from one month to another; these currents are obviously very unrealistic. We believe that a more complete GCM simulations that include the effect of tides and spatial and temporal variability of the wind should be carried out in order to uncover the origin of the scaling properties reported here.

Appendix A: The Scaling Properties of Upper Ocean Current Under the Action of Long-range Correlated Wind

[37] Here we analytically derive the power spectrum of upper ocean currents under the action of long-range correlated wind.

[38] Given equations (1)–(2) it is possible to perform a Fourier transform to obtain

$$\frac{\partial^2 \hat{g}(\omega, z)}{\partial z^2} - i\frac{\omega + f}{\nu}\hat{g}(\omega, z) = 0, \tag{A1}$$

where $\hat{g}(\omega, z) = \hat{u}(\omega, z) + i\hat{v}(\omega, z)$ and $\hat{u}$, $\hat{v}$ are the Fourier transform of the zonal and meridional currents, u, v. ω is the

frequency where we assume here that $\omega > 0$. The solution to equation (A1) is

$$\hat{g}(\omega, z) = Ae^{(1+i)z/d} + Be^{-(1+i)z/d}, \tag{A2}$$

where $d = \sqrt{2\nu/(\omega + f)}$ is equivalent to the conventional Ekman layer depth.

[39] It is possible to find the coefficients A, B of equation (A2) using the boundary conditions. Here we assume that at large depths the currents are constant, thus the Fourier transform of the currents for $z \to -\infty$ is zero (for $\omega > 0$) leading to $\hat{g}(\omega, z \to -\infty) = 0$. Thus $B = 0$. For the surface, $z = 0$, the boundary condition (3) holds leading to

$$\frac{\partial \hat{g}}{\partial z} \mid_{z=0} = \frac{1}{\rho_0 \nu}(\hat{\tau}^x + i\hat{\tau}^y), \tag{A3}$$

where $\hat{\tau}^x$ and $\hat{\tau}^y$ are the Fourier transform of the zonal and meridional wind stresses, τ^x and τ^y. From this relation we find A and obtain the following solution

$$\hat{g}(\omega, z) = \frac{d}{\sqrt{2}\rho_0 \nu}(\hat{\tau}^x + i\hat{\tau}^y)e^{z/d} \cdot [\cos(z/d + \pi/4) + i\sin(z/d + \pi/4)]. \tag{A4}$$

Thus,

$$\| \hat{g} \|^2 = \left(\frac{d}{\sqrt{2}\rho_0 \nu}\right)^2 \left(\| \hat{\tau}^x \|^2 + \| \hat{\tau}^y \|^2\right) e^{2z/d} = \| \hat{u} \|^2 + \| \hat{v} \|^2 . \tag{A5}$$

So far, we didn't assume any specific form of the wind stress.

[40] To find the scaling exponent of the simulate currents, $\beta_c(\omega)$, based on wind that follows a scaling law with a scaling exponent β_w for the wind speed, we assume the following: (1) the scaling of the wind stress is similar to the scaling of the wind, (2) the scaling of the square of the (wind/current) speed is similar to that of the speed itself, and (3) the power spectrum (both of winds and currents) of the zonal component is similar to the power spectrum of the meridional component (i.e., $\|\hat{\tau}^x\|^2 \sim \|\hat{\tau}^y\|^2$ and $\|\hat{u}\|^2 \sim \|\hat{v}\|^2$). Assumptions (1) and (2) are base on the conjecture that static transformation [i.e., $y_t = f(x_t)$ and $y_t \neq f(x_t, x_{t-1}, x_{t-2}, \ldots)$] does not drastically alter the temporal correlations. It follows from *Kalisky et al.* [2005] that if a time series, x, is a linear series that follows a scaling law $\|\hat{x}\|^2 \sim \omega^{-\beta_x}$ with $\beta_x > 0.5$, the scaling exponent of the square of the series, x^2 is $\beta_{x^2} = 2\beta_x - 1$. Then, using equation (A5) we obtain

$$\frac{1}{\omega^{\beta_c(\omega)}} \sim \frac{1}{(\omega + f)^2 \omega^{\beta_w}} e^{4z\sqrt{(\omega+f)/(2\nu)}}. \tag{A6}$$

This relation is plotted in Figure 6c (dashed line) using the parameter values that we use to simulate the current speed time series shown in Figure 5b; the agreement between the theoretical curve and the simulated curve seems reasonable. The differences between the two may be attribute to finite size effects, to the simplifying assumptions assumed above, and to generalization of $\beta_{x^2} = 2\beta_x - 1$ relation to time series with crossovers in the power spectrum.

[41] For the surface $z = 0$ equation (A6) leads to $\beta_c \to \beta_w + 2$ for $\omega \gg f$ and to $\beta_c \to \beta_w$ for $\omega \ll f$, supporting the observed crossover at $\omega \approx f$ with much larger scaling exponent at the high-frequency regime. For larger depths this crossover becomes even more pronounced due to the action of the exponential function in equation (A6), i.e., with suppressed high frequency and thus smoother currents. We observed these two characteristics for simulated currents from larger depths (data not shown).

[42] **Acknowledgments.** H.G. is the Incumbent Chair of the Rowland and Sylvia Schaefer Career Development and is supported by a research grant from the Estate of Sanford Kaplan. The Eilat Port Authority allowed us to install a high-frequency radar site in their area, and Airspan provides the wireless communication between the radar sites. We would also like to thank the management and the staff of the Inter-University Institute for Marine Sciences (IUI) of Eilat for their cooperation and help. We thank Dror Mirzayof for his help. This research was supported by the North Atlantic Treaty Organization grant SfP982220.

References

Ashkenazy, Y., P. C. h. Ivanov, S. Havlin, C.-K. Peng, A. L. Goldberger, and H. E. Stanley (2001), Magnitude and sign correlations in heartbeat fluctuations, *Phys. Rev. Lett.*, *86*, 1900–1903.

Ashkenazy, Y., D. R. Baker, H. Gildor, and S. Havlin (2003a), Nonlinearity and multifractality of climate change in the past 420,000 years, *Geophys. Res. Lett.*, *30*(22), 2146, doi:10.1029/2003GL018099.

Ashkenazy, Y., S. Havlin, P. C. h. Ivanov, C.-K. Peng, V. Schulte-Frohlinde, and H. E. Stanley (2003b), Magnitude and sign scaling in power-law correlated time series, *Physica A*, *323*, 19–41.

Barrick, D. E. (2002), Geometrical dilution of statistical accuracy (GDOSA) in multi-static HF radar networks, CODAR Ocean Sensors, *Tech. Rep.* (Available at http://www.codar.com/images/about/2006Barrick_GDOSA.pdf)

Barrick, D. E., B. J. Lipa, and R. D. Crissman (1985), Mapping surface currents with CODAR, *Sea Technol.*, *26*, 43–48.

Bartos, I., and I. M. Janosi (2006), Nonlinear correlations of daily temperature records over land, *Nonlinear Processes Geophys.*, *13*, 571–576.

Berman, T., N. Paldor, and S. Brenner (2003), The seasonality of tidal circulation in the Gulf of Elat, *Isr. J. Earth. Sci.*, *52*, 11–19.

Biton, E., J. Silverman, and H. Gildor (2008), Observations and modeling of pulsating density current, *Geophys. Res. Lett.*, *35*, L14603, doi:10.1029/2008GL034123.

Bunde, A., J. F. Eichner, S. Havlin, E. Koscielny-Bunde, H. J. Schellnhuber, and D. Vyushin (2004), Comment on "Scaling of atmosphere and ocean temperature correlations in observations and climate models", *Phys. Rev. Lett.*, *92*, 039801.

Ekman, V. W. (1905), On the influence of the Earth's rotation in ocean-currents, *Arch. Math. Astron. Phys.*, *2*, 1–52.

Fraedrich, K., and R. Blender (2003), Scaling of atmosphere and ocean temperature correlations in observations and climate models, *Phys. Rev. Lett.*, *90*, 108,501.

Fraedrich, K., U. Luksch, and R. Blender (2004), 1/*f*-Model for long time memory of the ocean surface temperature, *Phys. Rev. E*, *70*, 037,301-1.

Genin, A., and N. Paldor (1998), Changes in the circulation and current spectrum near the tip of the narrow, seasonally mixed Gulf of Elat, *Isr. J. Earth. Sci.*, *47*, 87–92.

Gildor, H., E. Fredj, J. Steinbuck, and S. Monismith (2009), Evidence for submesoscale barriers to mixing in the ocean from current measurements and aerial-photographs, *J. Phys. Oceanogr.*, doi:10.1175/2009JPO4116.1, in press.

Gill, A. E. (1982), *Atmosphere-Ocean Dynamics*, Elsevier, London.

Govindan, R. B., and H. Kantz (2004), Long-term correlations and multifractality in surface wind speed, *Europhys. Lett.*, *68*, 184–190.

Govindan, R. B., D. Vyushin, A. Bunde, S. Brenner, S. Havlin, and H. J. Schellnhuber (2002), Global climate models violate scaling of the observed atmospheric variability, *Physica Rev. Lett.*, *89*, 028,501.

Govindan, R. B., A. Bunde, and S. Havlin (2003), Volatility in atmospheric temperature variability, *Physica A*, *318*, 529–536.

Hurst, H. E. (1951), Long-term storage capacity of reservoirs, *Trans. Am. Soc. Civ. Eng.*, *116*, 770–808.

Huybers, P., and W. Curry (2006), Links between annual, Milankovitch and continuum temperature variability, *Nature*, *441*, 329–332.

Kalisky, T., Y. Ashkenazy, and S. Havlin (2005), Volatility of linear and nonlinear time series, *Phys. Rev. E*, *72*, 011,913.

Kantelhardt, J. W., S. A. Zschiegner, E. Koscielny-Bunde, S. Havlin, A. Bunde, and H. E. Stanley (2002), Multifractal Detrended Fluctuation Analysis of nonstationary time series, *Physica A*, *316*, 87–114.

Kantelhardt, J. W., E. Koscielny-Bunde, D. Rybski, P. Braun, A. Bunde, and S. Havlin (2006), Long-term persistence and multifractality of precipitation and river runoff records, *J. Geophys. Res.*, *111*, D01106, doi:10.1029/2005JD005881.

Kocak, K. (2008), Practical ways of evaluating wind speed persistence, *Energy*, *33*, 65–70.

Lekien, F., and H. Gildor (2009), Computation and approximation of the length scales of harmonic modes with application to the mapping of surface currents in the Gulf of Eilat, *J. Geophys. Res.*, doi:10.1029/2008JC004742, in press.

Livina, V., Y. Ashkenazy, Z. Kizner, V. Strygin, A. Bunde, and S. Havlin (2003), A stochastic model of river discharge fluctuations, *Physica A*, *330*, 283–290.

Makse, M., S. Havlin, M. Schwartz, and H. E. Stanley (1996), Method for generating long-range correlations for large systems, *Phys. Rev. E*, *53*, 5445–5449.

Manasrah, R. S., F. A. Al-horani, M. Y. Rasheed, S. A. Al-rousan, and M. A. Khalaf (2006), Patterns of summer vertical and horizontal currents in coastal waters of the northern Gulf of Aqaba, Red Sea, *Estuarine Coastal Shelf Sci.*, *69*, 567–579.

Mandelbrot, B. B., and J. R. Wallis (1969), Some long-run properties of geophysical records, *Water Resour. Res.*, *5*, 321–340.

Monismith, S. G., and A. Genin (2004), Tides and sea level in the Gulf of Aqaba (Eilat), *J. Geophys. Res.*, *109*, C04015, doi:10.1029/2003JC002069.

Pandey, G., S. Lovejoy, and D. Schertzer (1998), Multifractal analysis of daily river flows including extremes for basins of five to two million square kilometres, one day to 75 years, *J. Hydrol.*, *208*, 62–81.

Pelletier, J. D. (1997), Analysis and modeling of the natural variability of climate, *J. Clim.*, *10*, 1331–1342.

Peng, C.-K., S. Buldyrev, S. Havlin, M. Simons, H. E. Stanley, and A. L. Goldberger (1994), Mosaic organization of DNA nucleotides, *Phys. Rev. E*, *49*, 1685–1689.

Peng, C.-K., S. Havlin, H. E. Stanley, and A. L. Goldberger (1995), Quantification of scaling exponents and crossover phenomena in nonstationary time series, *Chaos*, *5*, 82–87.

Roman, H. E., A. Celi, and G. De-Filippi (2008), Fluctuation analysis of meteo-marine data, *Eur. Phys. J.*, *161*, 195–205.

Schreiber, T., and A. Schmitz (1996), Improved surrogate data for nonlinearity tests, *Phys. Rev. Lett.*, *77*, 635–638.

Schreiber, T., and A. Schmitz (2000), Surrogate time series, *Physica D*, *142*, 346–382.

Schulz, B. M., M. Schulz, and S. Trimper (2001), Wind direction and strength as a two-dimensional random walk, *Phys. Lett. A*, *291*, 87–91.

Tessier, Y., S. Lovejoy, P. Hubert, D. Schertzer, and S. Pecknold (1996), Multifractal analysis and modeling of rainfall and river flows and scaling, causal transfer functions, *J. Geophys. Res.*, *101*, 26,427–26,440.

Turcotte, D. L., and L. Greene (1993), A scale-invariant approach to flood-frequency analysis, *Stochastic Hydrol. Hydraul.*, *7*, 33–40.

Y. Ashkenazy, Department of Solar Energy and Environmental Physics, BIDR, Ben-Gurion University, Midreshet Ben-Gurion 84990, Israel. (ashkena@bgu.ac.il)

H. Gildor, Department of Environmental Sciences and Energy Research, Weizmann Institute of Science, Rehovot 76100, Israel.